Lindhard function - charge and spin susceptibility of free electron gas

① Linear response - reminder

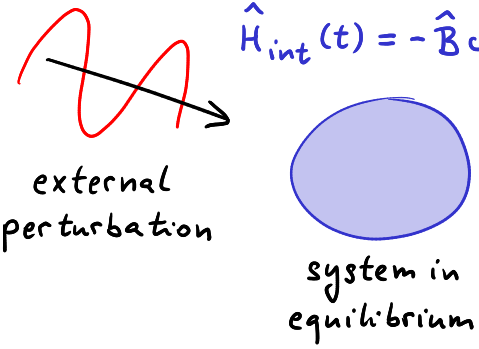

- linear susceptibility & Kubo formula

$$\langle A \rangle_t = \langle A \rangle_{eq} + \int_{-\infty}^{\infty} \chi(t,t')\,\varphi(t')\,dt' \qquad \chi(t,t') = \frac{i}{\hbar}\langle [\hat{A}(t), \hat{B}(t')] \rangle_{eq}\,\vartheta(t-t')$$

equilibrium system → homogeneity in time $\chi(t,t') = \chi(t-t')$

in Fourier domain $\langle A \rangle_\omega = \chi(\omega)\varphi(\omega)$ with $\chi(\omega) = \frac{i}{\hbar}\int_{-\infty}^{\infty} dt\; e^{i(\omega+i0^+)t}\langle [\hat{A}(t), \hat{B}] \rangle_{eq}\,\vartheta(t)$

(2) Free-electron gas

- ionic background considered homogeneous and ignored
- Coulomb interactions among electrons ignored → independent electrons

Hamiltonian $\hat{H} = \sum_{k\sigma} \varepsilon_k \hat{c}^{+}_{k\sigma} \hat{c}_{k\sigma}$ dispersion $\varepsilon_k = \frac{\hbar^2 k^2}{2m}$

Born-von Kármán boundary conditions applied to volume V → compatible $\bar{k}$ vectors

normalized eigenstate wave functions $\Psi_k(\bar{r}) = \frac{1}{\sqrt{V}} e^{i\bar{k}\cdot\bar{r}}$ ⊗ spin ↑ or ↓

N electrons in volume V, i.e. electron density $n = \frac{N}{V}$

Fermi sphere – lowest N electron states in $\bar{k}$-space

Fermi radius $k_F = (3\pi^2 n)^{\frac{1}{3}}$ ← $\frac{4}{3}\pi k_F^3 = N \cdot \underbrace{\frac{(2\pi)^3}{V}}_{\text{volume per compatible } \bar{k}} \cdot \frac{1}{2}$

Fermi level $E_F = \frac{\hbar^2 k_F^2}{2m}$

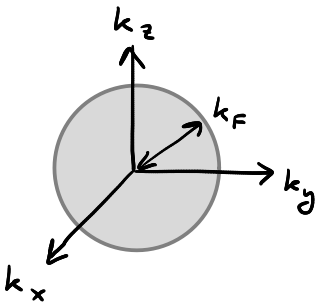

③ Charge susceptibility

- electron density $\hat{n}(\bar{r}) = \sum_q e^{i\bar{q}\cdot\bar{r}}\,\hat{n}_q \leftarrow \hat{n}_q = \frac{1}{V}\sum_{kG}\hat{c}^+_{kG}\,\hat{c}_{k+q\,G}$

  charge density $\hat{\rho}(\bar{r}) = \sum_q e^{i\bar{q}\cdot\bar{r}}\,\hat{\rho}_q \leftarrow \hat{\rho}_q = -e\,\frac{1}{V}\sum_{kG}\hat{c}^+_{kG}\,\hat{c}_{k+q\,G}$

coupling to external scalar potential $\varphi(\bar{r},t) = \sum_q e^{i\bar{q}\cdot\bar{r}}\,\varphi_q(t)$ provided by the interaction Hamiltonian $\hat{H}_{int}(t) = -\int d^3\bar{r}\;\hat{\rho}(\bar{r})\,\varphi(\bar{r}) = -V\sum_q \hat{\rho}_{-q}\,\varphi_q(t)$

- charge susceptibility

$$\chi_{ch}(\bar{q},t) = \frac{i}{\hbar}V\langle[\hat{\rho}_q(t),\hat{\rho}_{-q}]\rangle\,\vartheta(t) \qquad \langle\rho_q\rangle_t = \int dt'\,\chi_{ch}(q,t-t')\,\varphi_q(t')$$

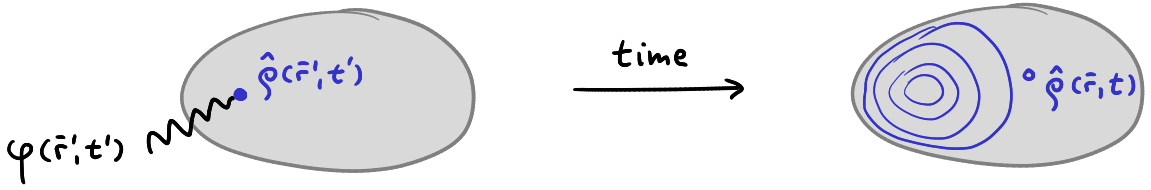

intuitive picture of real-space $\chi_{ch}(\bar{r}-\bar{r}',t-t')$

- Why $[\hat{\rho}_q, \hat{\rho}_{-q}]$ and not $\bar{q}, \bar{q}$ or general $\bar{q}, \bar{q}'$?

translational invariance – momentum is conserved

$\hat{\rho}_q$ and $\hat{\rho}_{-q}$ are conjugate: $\hat{\rho}_q^\dagger = \left[\frac{1}{V}\int d^3\bar{r}\; e^{-i\bar{q}\cdot\bar{r}}\hat{\rho}(\bar{r})\right]^\dagger = \frac{1}{V}\int d^3\bar{r}\; e^{i\bar{q}\cdot\bar{r}}\hat{\rho}^\dagger(\bar{r}) = \hat{\rho}_{-q}$

hermitian $= \hat{\rho}(\bar{r})$

$\hat{\rho}_{-q}$ transfers momentum $\bar{q}$ to the system, $\hat{\rho}_q$ extracts $\bar{q}$ back out of the system

- explicit form of retarded χ_{ch}

$$\chi_{ch}(\bar{q},t) = (-e)^2 \frac{1}{V}\frac{i}{\hbar}\left\langle \left[\sum_{k\sigma} \hat{c}^\dagger_{k\sigma}(t)\,\hat{c}_{k+q\sigma}(t)\;,\; \sum_{k'\sigma'} \hat{c}^\dagger_{k'\sigma'}\,\hat{c}_{k'-q,\sigma'} \right] \right\rangle \vartheta(t)$$

$$\chi_{ch}(\bar{q},\omega) = \int_{-\infty}^{\infty} dt\; e^{i(\omega+i0^+)t}\,\chi_{ch}(\bar{q},t)$$

For free-electron gas (or non-interacting electrons in general)

$$\chi_{ch}(\bar{q},\omega) = (-e)^2\,\Pi_0(\bar{q},\omega)$$

Lindhard function

Jens Lindhard
(1922-1997)

https://brugere.lex.dk/1646

- evalnation of Lindhasd function

$$\Pi_0(\bar{q},t) = \frac{1}{V}\frac{i}{\hbar}\left\langle \left[\sum_{kG} \hat{c}^{+}_{kG}(t)\,\hat{c}_{k+qG}(t),\ \sum_{k'G'} \hat{c}^{+}_{k'G'}\,\hat{c}_{k'-q,G'} \right] \right\rangle \vartheta(t)$$

Heisenberg operators

$$\hat{c}^{+}_{kG}(t) = e^{\frac{i}{\hbar}\hat{H}t}\,\hat{c}^{+}_{kG}\,e^{-\frac{i}{\hbar}\hat{H}t} = e^{\frac{i}{\hbar}\varepsilon_k t}\,\hat{c}^{+}_{kG} \qquad \hat{c}_{kG}(t) = e^{-\frac{i}{\hbar}\varepsilon_k t}\,\hat{c}_{kG}$$

↑ energy increased by ε_k

$$\Pi_0(\bar{q},t) = \frac{1}{V}\frac{i}{\hbar}\sum_{kk'}\sum_{GG'} e^{\frac{i}{\hbar}(\varepsilon_k-\varepsilon_{k+q})t} \left\langle \hat{c}^{+}_{kG}\,\hat{c}_{k+qG}\,\hat{c}^{+}_{k'G'}\,\hat{c}_{k'-qG'} - \hat{c}^{+}_{k'G'}\,\hat{c}_{k'-qG'}\,\hat{c}^{+}_{kG}\,\hat{c}_{k+qG} \right\rangle$$

$\delta_{q,0}$ $\qquad$ $\delta_{q,0}$

$\delta_{k,k'-q}\,\delta_{k+q,k'}\,\delta_{GG'}$ $\qquad$ $\delta_{k',k+q}\,\delta_{k'-q,k}\,\delta_{GG'}$

$$\langle \cdots \rangle = \begin{cases} \langle GS|\cdots|GS\rangle & T=0 \\ \sum_n \frac{e^{-\beta E_n}}{Z}\langle n|\cdots|n\rangle & T>0 \end{cases}$$

$$\Pi_0(\bar{q},t) = \frac{1}{V}\frac{i}{\hbar}\sum_{kk'}\sum_{GG'} e^{\frac{i}{\hbar}(\varepsilon_k-\varepsilon_{k+q})t}\left\langle \hat{c}^+_{kG}\hat{c}_{k+qG}\hat{c}^+_{k'G'}\hat{c}_{k'-qG'} - \hat{c}^+_{k'G'}\hat{c}_{k'-qG'}\hat{c}^+_{kG}\hat{c}_{k+qG}\right\rangle$$

$$\frac{1}{V}\frac{i}{\hbar}\delta_{q,0}\left\langle \left(\sum_{kG}\hat{c}^+_{kG}\hat{c}_{kG}\right)\left(\sum_{k'G'}\hat{c}^+_{k'G}\hat{c}_{k'G'}\right) - \left(\sum_{k'G'}\hat{c}^+_{k'G}\hat{c}_{k'G'}\right)\left(\sum_{kG}\hat{c}^+_{kG}\hat{c}_{kG}\right)\right\rangle \quad \text{static 0}$$

$$\frac{1}{V}\frac{i}{\hbar}\sum_{kG} e^{\frac{i}{\hbar}(\varepsilon_k-\varepsilon_{k+q})t}\left\langle \hat{c}^+_{kG}\hat{c}_{k+qG}\hat{c}^+_{k+qG}\hat{c}_{kG} - \hat{c}^+_{k+qG}\hat{c}_{kG}\hat{c}^+_{kG}\hat{c}_{k+qG}\right\rangle$$

nonzero $\bar{q}$: $\quad \hat{n}_{kG}(1-\hat{n}_{k+qG}) \qquad \hat{n}_{k+q,G}(1-\hat{n}_{kG}) \rightarrow \hat{n}_{kG}-\hat{n}_{k+qG}$

zero $\bar{q}$ special → zero value

Fourier transform $\quad \frac{i}{\hbar}\int_0^\infty dt\; e^{\frac{i}{\hbar}(\varepsilon_k-\varepsilon_{k+q})t}\, e^{i(\omega+i0^+)t} = \frac{-1}{\varepsilon_k-\varepsilon_{k+q}+\hbar\omega+i0^+}$

$$\Pi_0(\bar{q},\omega) = \frac{1}{V}\sum_{kG}\frac{n_{kG}-n_{k+qG}}{\varepsilon_{k+q}-\varepsilon_k-\hbar\omega-i0^+} = \frac{2}{V}\sum_k \frac{n_F(\varepsilon_k)-n_F(\varepsilon_{k+q})}{\varepsilon_{k+q}-\varepsilon_k-\hbar\omega-i0^+} \qquad \text{for finite } T$$

- a different view on the intermediate result

$$\frac{1}{V}\frac{i}{\hbar}\sum_{k\sigma} e^{\frac{i}{\hbar}(\varepsilon_k-\varepsilon_{k+q})t}\left\langle \hat{c}^+_{k\sigma}\hat{c}_{k+q\sigma}\,\hat{c}^+_{k+q\sigma}\hat{c}_{k\sigma} - \hat{c}^+_{k+q\sigma}\hat{c}_{k\sigma}\,\hat{c}^+_{k\sigma}\hat{c}_{k+q\sigma}\right\rangle$$

$$= \frac{1}{V}\frac{i}{\hbar}\sum_{k\sigma}\left\langle \hat{c}^+_{k\sigma}(t)\,\hat{c}_{k+q\sigma}(t)\,\hat{c}^+_{k+q\sigma}\hat{c}_{k\sigma} - \hat{c}^+_{k+q\sigma}\hat{c}_{k\sigma}\,\hat{c}^+_{k\sigma}(t)\,\hat{c}_{k+q\sigma}(t)\right\rangle$$

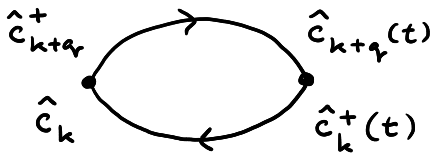

$\hat{\rho}_{-q}$ $\quad$ $\hat{\rho}_q(t)$

product of two propagators ?

$$\langle \hat{c}^+_{k\sigma}(t)\,\hat{c}_{k\sigma}\rangle\langle \hat{c}_{k+q\sigma}(t)\,\hat{c}^+_{k+q\sigma}\rangle$$

$$-\langle \hat{c}_{k\sigma}\,\hat{c}^+_{k\sigma}(t)\rangle\langle \hat{c}^+_{k+q\sigma}\,\hat{c}_{k+q\sigma}(t)\rangle$$

(4) Spin susceptibility

- magnetic moment density associated with electron spins

$$\hat{m}_\alpha(\vec{r}) = \sum_q e^{i\vec{q}\cdot\vec{r}}\,\hat{m}_{\alpha q} \qquad \hat{m}_{\alpha q} = -\frac{1}{V} g\mu_B \frac{1}{2} \sum_k \sum_{ss'} \hat{c}^+_{ks}\,\sigma^\alpha_{ss'}\,c_{k+q\,s'} = -g\mu_B \hat{S}^\alpha_q$$

Pauli matrices $\sigma^x = \begin{pmatrix} 0 & 1 \\ 1 & 0 \end{pmatrix}$ $\sigma^y = \begin{pmatrix} 0 & -i \\ i & 0 \end{pmatrix}$ $\sigma^z = \begin{pmatrix} 1 & 0 \\ 0 & -1 \end{pmatrix}$

$\rightarrow$ $m_z \sim c^+_{k\uparrow} c_{k+q\uparrow} - c^+_{k\downarrow} c_{k+q\downarrow}$ $\qquad m_x \sim \hat{c}^+_{k\uparrow} \hat{c}_{k+q\downarrow} + \hat{c}^+_{k\downarrow} \hat{c}_{k+q\uparrow}$

- interaction with external magnetic field $\hat{H}_{int}(t) = -V \sum_{q\alpha} \hat{m}_{\alpha,-q}\, B_{\alpha q}(t)$

- spin susceptibility

$$\chi^{\alpha\beta}(\vec{q},t) = \frac{i}{\hbar} V \langle [\hat{S}^\alpha_q(t), \hat{S}^\beta_{-q}] \rangle\, \vartheta(t) \qquad \chi^{\alpha\beta}(\vec{q},\omega) = \int_{-\infty}^{\infty} dt\, e^{i(\omega+i0^+)t}\, \chi^{\alpha\beta}(\vec{q},t)$$

For an isotropic system : $\chi_{\alpha\beta} = \chi\,\delta_{\alpha\beta}$

(no magnetic ordering, spin-isotropic or spin-insensitive interactions)

- magnetic susceptibility $(g\mu_B)^2 \chi^{\alpha\beta}$

- charge and spin susceptibility for independent electrons – comparison

$$\langle [\hat{\rho}_q(t), \hat{\rho}_{-q}(t)] \rangle \sim \sum_{kk'} \langle [\hat{c}^+_{k\uparrow}(t)\hat{c}_{k+q\uparrow}(t) + \hat{c}^+_{k\downarrow}(t)\hat{c}_{k+q\downarrow}(t),\ \hat{c}^+_{k'\uparrow}\hat{c}_{k'-q\uparrow} + \hat{c}^+_{k'\downarrow}\hat{c}_{k'-q\downarrow}] \rangle$$

$$\langle [\hat{S}^x_q(t), \hat{S}^x_{-q}] \rangle \sim \sum_{kk'} \langle [\hat{c}^+_{k\uparrow}(t)\hat{c}_{k+q\downarrow}(t) + \hat{c}^+_{k\downarrow}(t)\hat{c}_{k+q\uparrow}(t),\ \hat{c}^+_{k'\uparrow}\hat{c}_{k'-q\downarrow} + \hat{c}^+_{k'\downarrow}\hat{c}_{k'-q\uparrow}] \rangle$$

(2) (1)

$$\langle [\hat{S}^\alpha_q(t), \hat{S}^\beta_{-q}] \rangle \sim \sum_{kk'} \sum_{s_1 \dots s_4} \langle [\hat{c}^+_{ks_1}(t)\, \sigma^\alpha_{s_1 s_2} \hat{c}_{k+q\, s_2}(t),\ \hat{c}^+_{k's_3}\, \sigma^\beta_{s_3 s_4} \hat{c}_{k'-q\, s_4}] \rangle$$

$$= \sum_k \underbrace{\sum_{ss'} \sigma^\alpha_{ss'} \sigma^\beta_{s's}}_{\mathrm{Tr}\,\sigma^\alpha\sigma^\beta = 2\delta_{\alpha\beta}} \underbrace{\langle [\hat{c}^+_{ks}(t)\, \hat{c}_{k+q\,s'}(t),\ \hat{c}^+_{k+q\,s'}\hat{c}_{ks}] \rangle}_{\text{independent on } s,s'}$$

conclusions: $\chi_{ch} = (-e)^2 \Pi_0 \qquad \chi^{\alpha\beta} = \delta_{\alpha\beta} \frac{1}{4} \Pi_0$

⑤ Explicit evaluation of Lindhard function for quadratic dispersion

$$\Pi_0(\bar{q},\omega) = \frac{2}{V}\sum_k \frac{n_F(\varepsilon_k) - n_F(\varepsilon_{k+q})}{\varepsilon_{k+q} - \varepsilon_k - \hbar\omega - i0^+}$$

evaluated for the dispersion $\varepsilon_k = \frac{\hbar^2 k^2}{2m} - E_F$

consider $T=0$ $\rightarrow$ $n_k - n_{k+q} = \begin{cases} +1 & k < k_F,\ |\bar{k}+\bar{q}| > k_F \\ -1 & k > k_F,\ |\bar{k}+\bar{q}| < k_F \\ 0 & \text{otherwise} \end{cases}$

$$\Pi_0(q,\omega) = \underbrace{\frac{2}{V}\sum_{\substack{k<k_F \\ |\bar{k}+\bar{q}|>k_F}} \frac{1}{\varepsilon_{k+q} - \varepsilon_k - \hbar\omega - i0^+}}_{F(\bar{q},\hbar\omega+i0^+)} - \underbrace{\frac{2}{V}\sum_{\substack{k>k_F \\ |\bar{k}+\bar{q}|<k_F}} \frac{1}{\varepsilon_{k+q} - \varepsilon_k - \hbar\omega - i0^+}}_{F(-\bar{q},-\hbar\omega-i0^+)}$$

by substitution

$\bar{k}+\bar{q} \rightarrow \bar{k}'$

$\bar{k} \rightarrow \bar{k}' - \bar{q}$

conversion to integrals

$$\frac{1}{V}\sum_k = \frac{1}{V}\frac{1}{\frac{(2\pi)^3}{V}}\int d^3\bar{k} = \frac{1}{(2\pi)^3}\int d^3\bar{k}$$

reduced variables for convenience $\bar{K} = \frac{\bar{k}}{2k_F}$ $\bar{Q} = \frac{\bar{q}}{2k_F}$ $W = \frac{\hbar\omega}{4E_F}$

integral evaluated in cylindrical coordinates with K_z along $\bar{Q}$ & via Sochocki-Plemelj

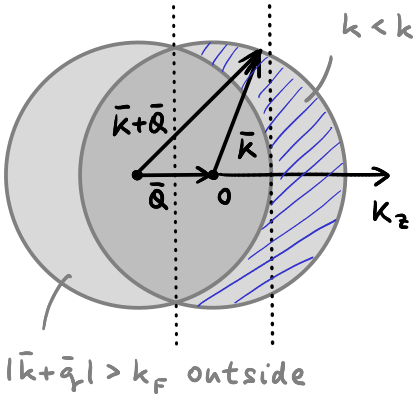

$$\int d^3\bar{K}\ \boxtimes = \int_{-\frac{Q}{2}}^{\frac{1}{2}-Q} dK_z \int_{\sqrt{\frac{1}{4}-(K_z+Q)^2}}^{\sqrt{\frac{1}{4}-K_z^2}} dK_r\, K_r \int_0^{2\pi} d\varphi\ \boxtimes + \dots$$

$K < \frac{1}{2}$

$|\bar{K}+\bar{Q}| > \frac{1}{2}$

$$\varepsilon_{k+q} - \varepsilon_k \sim (\bar{K}+\bar{Q})^2 - \bar{K}^2 = 2\bar{K}\cdot\bar{Q} + Q^2 = 2K_zQ + Q^2$$

$$\mathrm{Re}\,\Pi_0 = \frac{mk_F}{2\pi^2\hbar^2}\left\{1 + \frac{1}{4Q}\left[1-(Q-\frac{W}{Q})^2\right]\ln\left|\frac{W-Q^2-Q}{W-Q^2+Q}\right| + \frac{1}{4Q}\left[1-(Q+\frac{W}{Q})^2\right]\ln\left|\frac{W+Q^2+Q}{W+Q^2-Q}\right|\right\}$$

$$\mathrm{Im}\,\Pi_0(Q, W>0) = \frac{mk_F}{2\pi^2\hbar^2}\cdot\begin{cases} \frac{\pi}{Q}W & W < Q-Q^2 \\ \frac{\pi}{4Q}\left[1-(Q-\frac{W}{Q})^2\right] & |Q-Q^2| < W < Q+Q^2 \\ 0 & \text{otherwise} \end{cases}$$

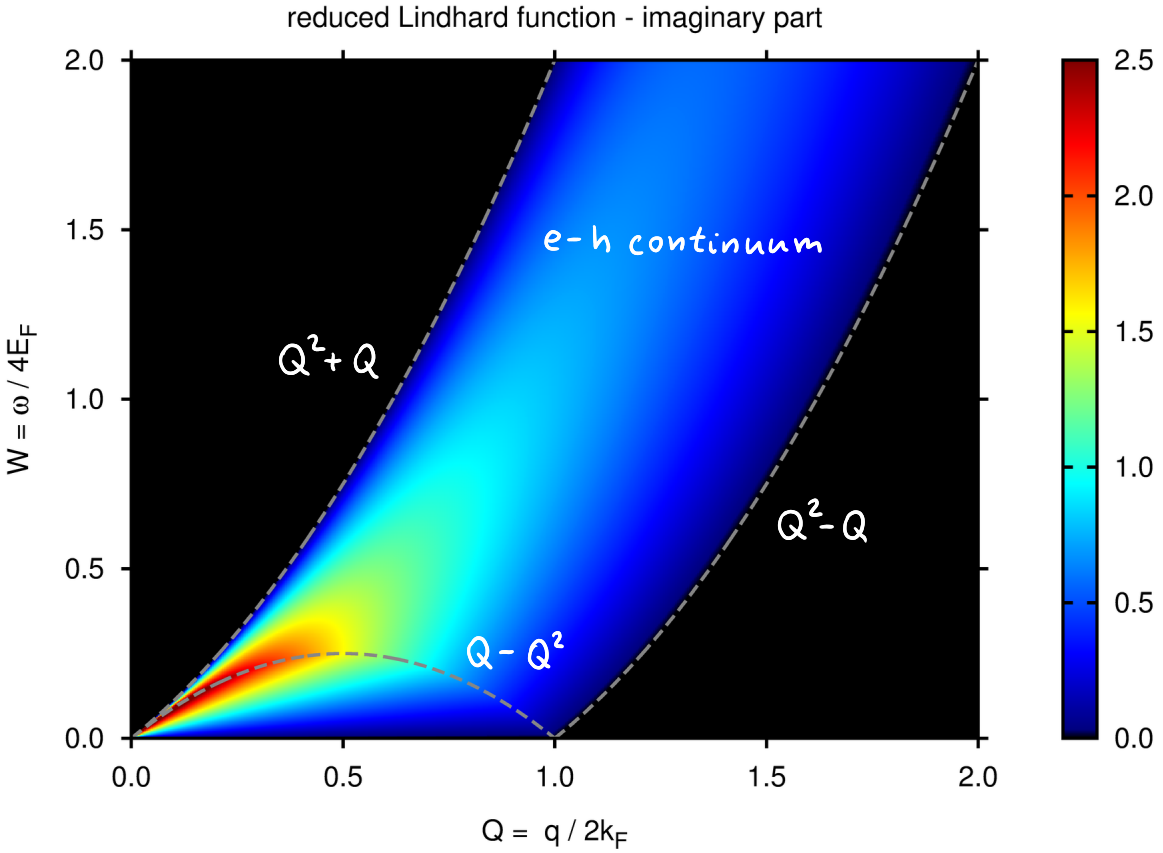
reduced Lindhard function - imaginary part
e-h continuum
Q^2+Q
Q^2-Q
$Q-Q^2$
$W = \omega / 4E_F$
$Q = q / 2k_F$
0.0
0.5
1.0
1.5
2.0
2.5

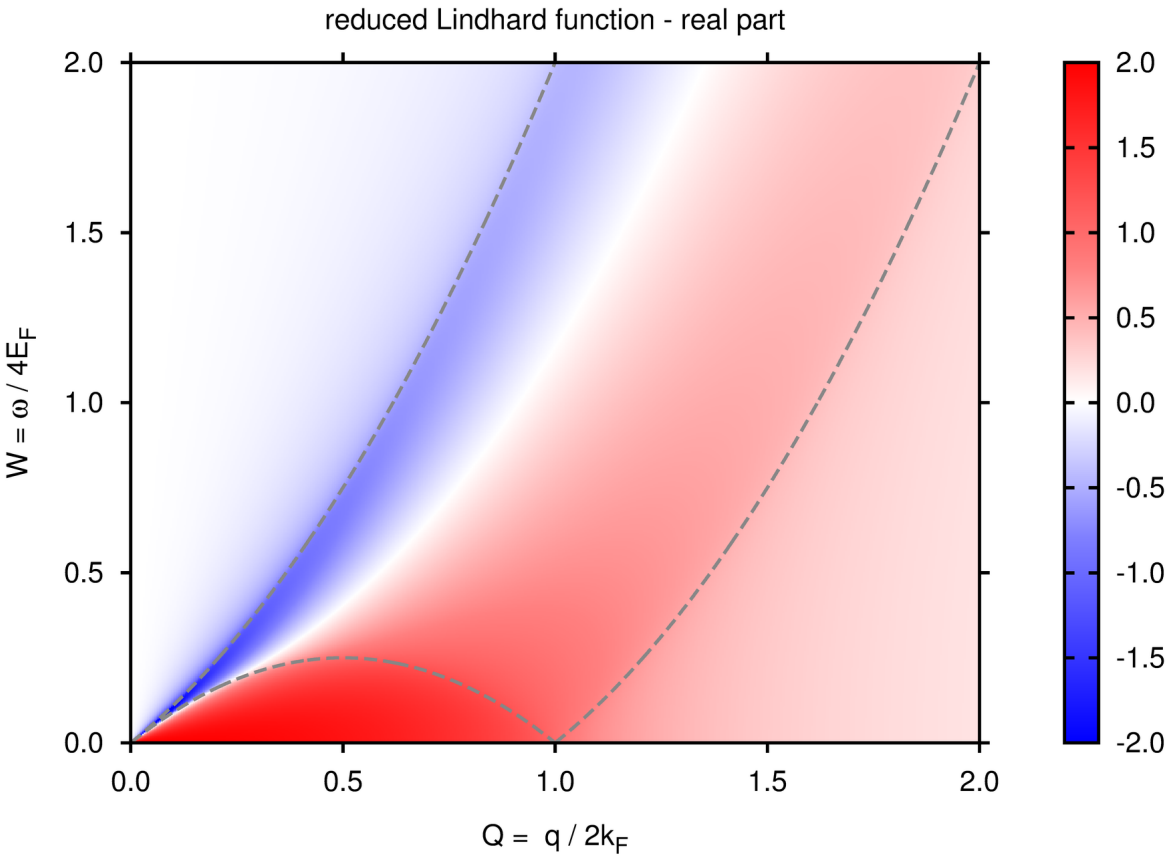
reduced Lindhard function - real part
2.0
1.5
1.0
0.5
0.0
W = ω / 4E_F
0.0
0.5
1.0
1.5
2.0
Q = q / 2k_F
2.0
1.5
1.0
0.5
0.0
-0.5
-1.0
-1.5
-2.0

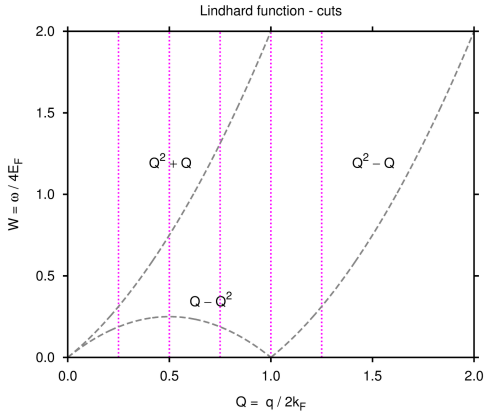
Lindhard function - cuts
W = ω / 4E_F
Q = q / 2k_F
Q^2 + Q
Q^2 – Q
Q – Q^2
0.0
0.5
1.0
1.5
2.0

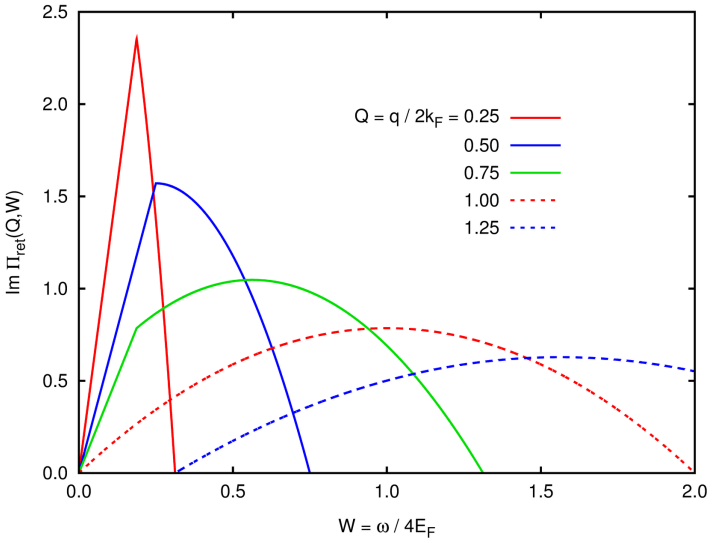
Im Π_ret(Q,W)
W = ω / 4E_F
Q = q / 2k_F = 0.25
0.50
0.75
1.00
1.25
0.0
0.5
1.0
1.5
2.0
2.5

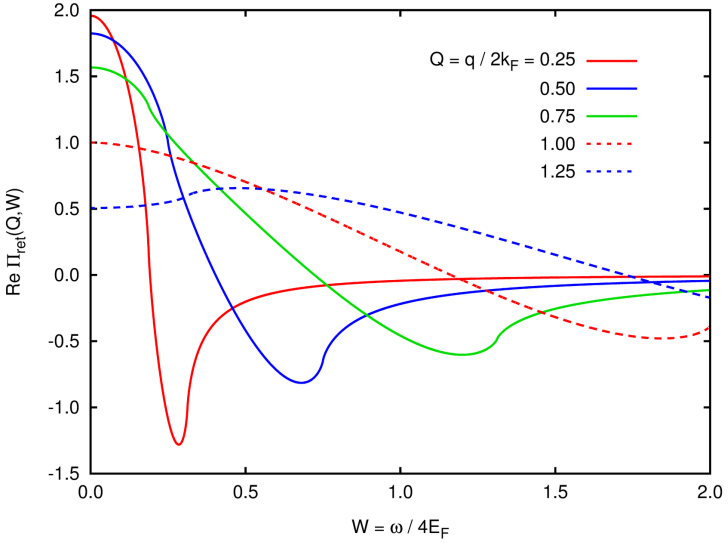
Re Π_ret(Q,W)
W = ω / 4E_F
Q = q / 2k_F = 0.25
0.50
0.75
1.00
1.25
-1.5
-1.0
-0.5
0.0
0.5
1.0
1.5
2.0

(6) Static limit $\omega \to 0$, RKKY interaction

- static Π_0 obtained by setting $\omega = 0$

$$\Pi_0(Q, \omega=0) = \frac{m k_F}{2\pi^2 \hbar^2}\left[1 + \frac{1-Q^2}{2Q} \ln\left|\frac{1+Q}{1-Q}\right|\right] \qquad \text{containing} \sim \frac{1-Q}{2Q}\ln|1-Q|$$

singular derivative at $Q = 1$ ($q = 2k_F$) $\sim \ln|1-Q|$

$\to$ $2k_F$ oscillations in real-space counterpart (Friedel oscillations) $\lambda = \frac{\pi}{k_F}$

$$\Pi_0(r, \omega=0) \sim \frac{1}{r^4}\left[2k_F r \cos(2k_F r) - \sin(2k_F r)\right]$$

- RKKY interaction (Ruderman - Kittel - Kasuya - Yosida)

localized moments interacting via spin-polarization of electron gas

$$\hat{H} = -J_{loc}\left[\sum_\alpha \hat{S}_1^\alpha \hat{G}^\alpha(\vec{r}_1) + \sum_\beta \hat{S}_2^\beta \hat{G}^\beta(\vec{r}_2)\right] + \hat{H}_{\text{cond. band}}$$

conduction-band spins: $\chi^{\alpha\beta}(\vec{r}_1 - \vec{r}_2, \omega=0) = \delta_{\alpha\beta}\chi(\Delta\vec{r}, \omega=0)$

$\to$ eff. interaction $-J\,\vec{S}_1 \cdot \vec{S}_2$ with $J \sim J_{loc}^2\,\chi(\Delta\vec{r}, \omega=0)$

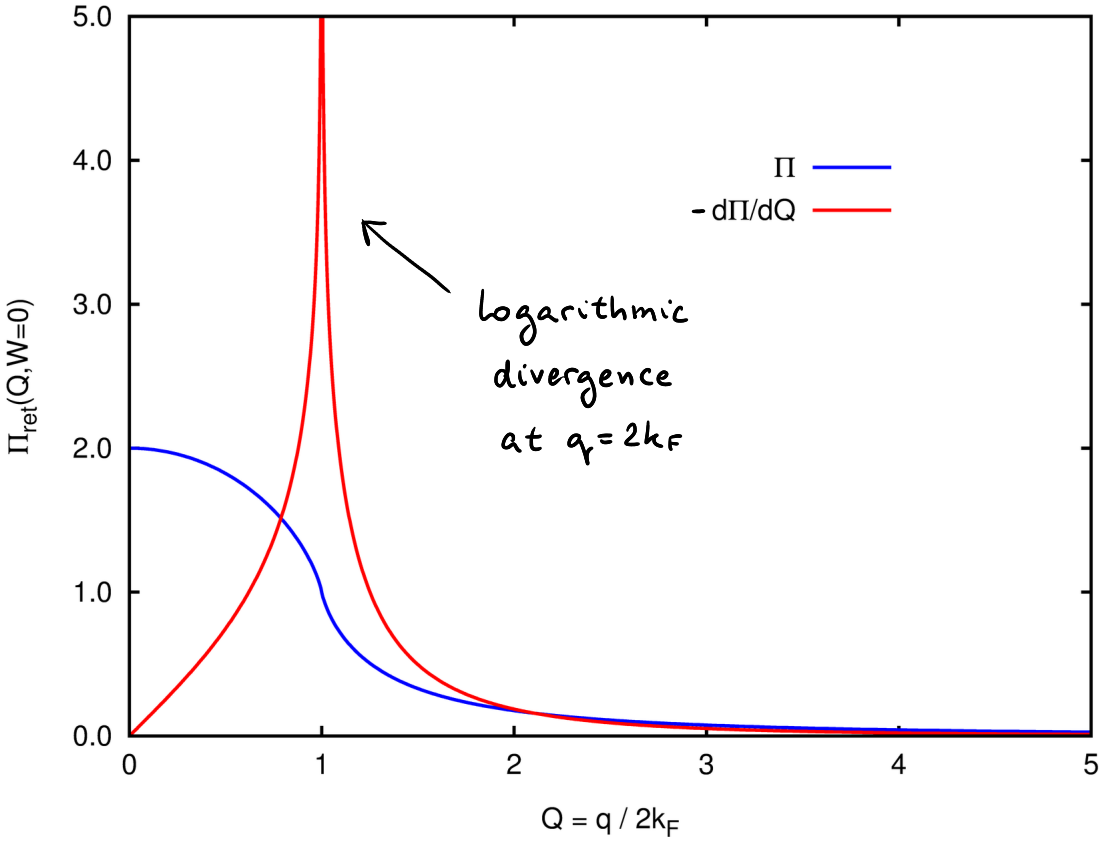
5.0
4.0
3.0
2.0
1.0
0.0
0
1
2
3
4
5
$\Pi_{ret}(Q, W=0)$
$Q = q / 2k_F$
Π
$-d\Pi/dQ$
Logarithmic
divergence
at $q = 2k_F$

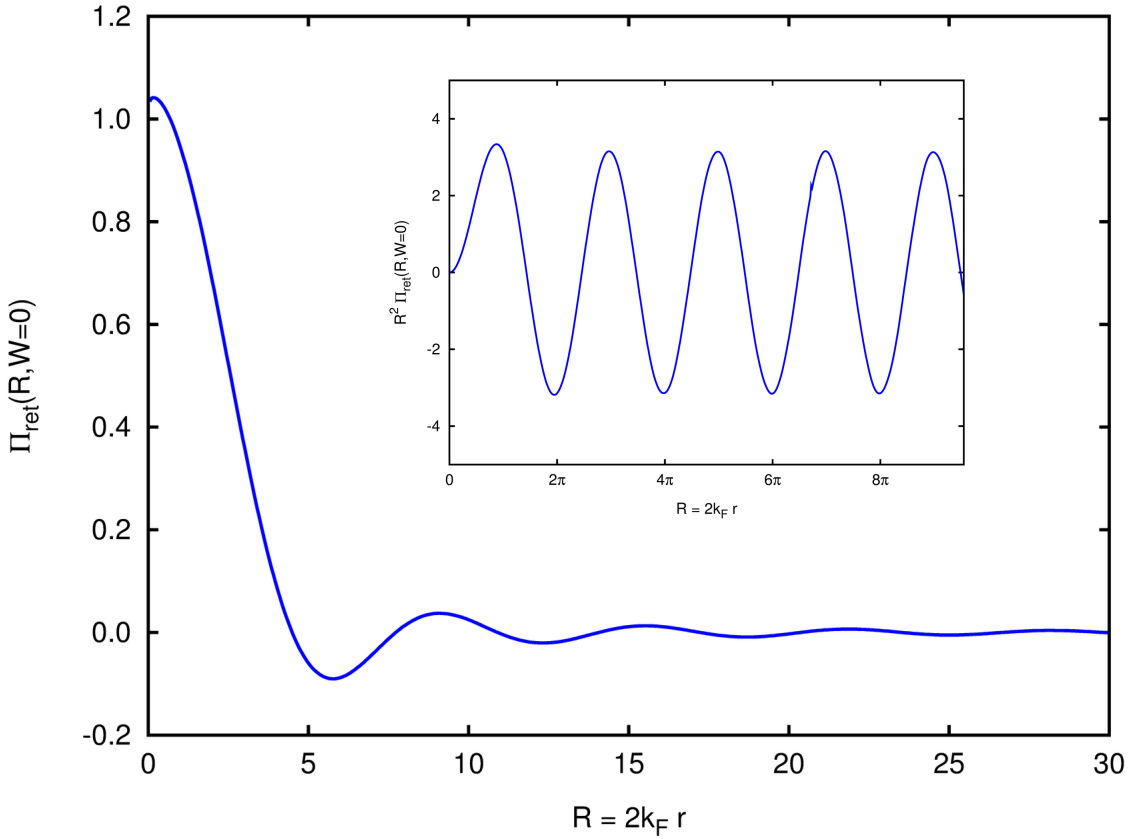
1.2
1.0
0.8
0.6
0.4
0.2
0.0
-0.2
0
5
10
15
20
25
30
$\Pi_{ret}(R,W=0)$
$R = 2k_F\, r$
4
2
0
-2
-4
0
2π
4π
6π
8π
$R^2\, \Pi_{ret}(R,W=0)$
$R = 2k_F\, r$

Revealing Magnetic Interactions from Single-Atom Magnetization Curves

Focko Meier,* Lihui Zhou, Jens Wiebe,† Roland Wiesendanger

The miniaturization of magnetic devices toward the limit of single atoms calls for appropriate tools to study their magnetic properties. We demonstrate the ability to measure magnetization curves of individual magnetic atoms adsorbed on a nonmagnetic metallic substrate with use of a scanning tunneling microscope with a spin-polarized tip. We can map out low-energy magnetic interactions on the atomic scale as evidenced by the oscillating indirect exchange between a Co adatom and a nanowire on Pt(111). These results are important for the understanding of variations that are found in the magnetic properties of apparently identical adatoms because of different local environments.

Magnetic nanostructures consisting of a few atoms on nonmagnetic substrates (adatoms) are explored as model systems for miniaturized data storage and spintronic devices and for the implementation of quantum computing. Because these structures are well defined and controllable on the atomic scale, they are ideally suited to study the fundamentals of magnetic interactions that are the ingredients of today's and future memory and computation technology.

Since the early days of modern research in magnetism, the magnetization in response to an external magnetic field (a magnetization curve) has been recorded to gather information on the basic properties of magnetic samples (*1*). Such curves can be used to deduce the sample's magnetic moment and magnetic anisotropy energy. The downscaling of samples from bulk over thin films and nanowires to nanodots requires an ever-increasing sensitivity of this method. It has been demonstrated that x-ray absorption spectroscopy with polarization analysis is able to measure magnetization curves of adatoms on a nonmagnetic substrate, albeit limited to large ensembles (*2*). Different approaches are potentially able to detect individual spins with nanometer spatial resolution ranging from magnetic resonance measurements (*3*) over magnetic exchange force microscopy (*4*) to scanning tunneling microscopy and spectroscopy (STM and STS) (*5*–*10*). Spin-averaged STS has been used to indirectly deduce the properties of single and coupled spins via the Kondo effect (*5*), the detection of noise (*6*, *7*), or the observation of exchange splittings (*8*, *9*). Inelastic electron tunneling has been adopted to measure the magnetic moments and anisotropy of individual atoms by spin-flip spectroscopy (*10*). This approach is complementary to the detection of magnetization curves but does not provide information on the dynamics of the spin and is so far restricted to adatoms on insulating layers. The method of choice for various substrates, spin-polarized STS (SP-STS), has been proven to detect single spins stabilized by direct exchange to

Institute of Applied Physics and Microstructure Research Center, University of Hamburg, Jungiusstrasse 11, D-20355 Hamburg, Germany.

*Present address: Laboratory of Atomic and Solid State Physics, Department of Physics, Cornell University, Ithaca, NY 14853, USA.

†To whom correspondence should be addressed. E-mail: jwiebe@physnet.uni-hamburg.de

F. Meier, L. Zhou, J. Wiebe, R. Wiesendanger, Science 320, 82 (2008)

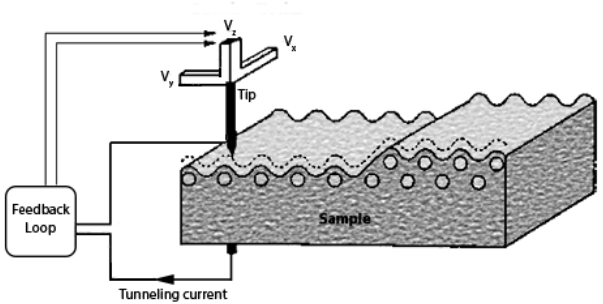

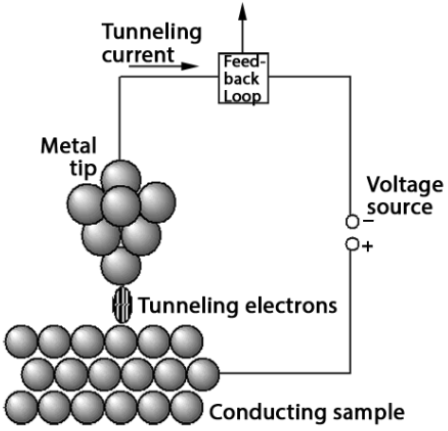

Fig. 2. Spin-polarized d*I*/d*V* curves from individual Co adatoms. (**A**) Curves measured on an hcp and on an fcc adatom by using the same tip as in fig. S1 with $\vec{B}$ as indicated (averages from six single curves, fcc curves are offset for clarity). The time-averaged magnetization of the adatoms $\langle \vec{M}_A \rangle$ is aligned with $\vec{B}$, resulting in a change in the d*I*/d*V* curve depending on the relative orientation of $\langle \vec{M}_A \rangle$ and $\vec{M}_T$ as indicated. a.u., arbitrary units. (Inset) Topograph colorized with simultaneously recorded d*I*/d*V* map at V_{stab} = −0.1 V of an area with two hcp (orange) and two fcc (blue) adatoms. (**B**) Magnetic asymmetry (A_{magn}) calculated from the curves of (A). (Tunneling parameters are as follows: I_{stab} = 1 nA, V_{stab} = 0.6 V, V_{mod} = 10 mV, T = 0.3 K.)

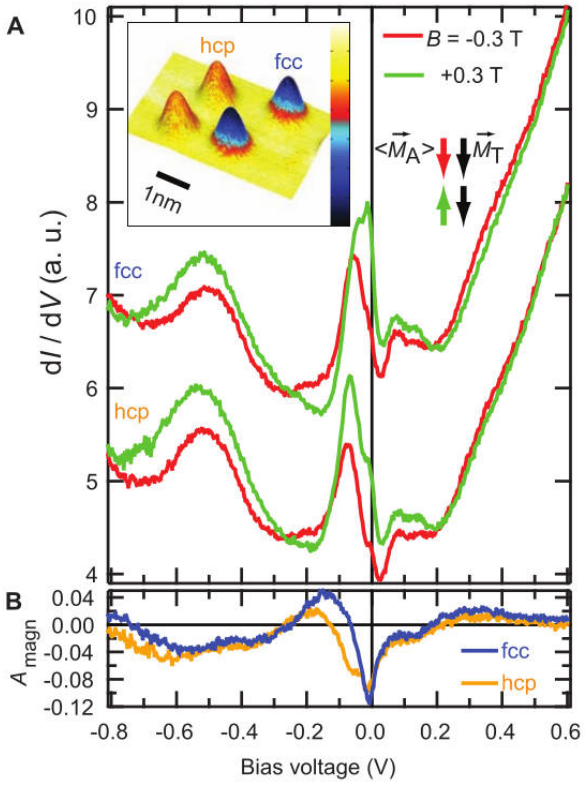

https://www.nanoscience.com/techniques/scanning-tunneling-microscopy/

F. Meier, L. Zhou, J. Wiebe, R. Wiesendanger, Science 320, 82 (2008)

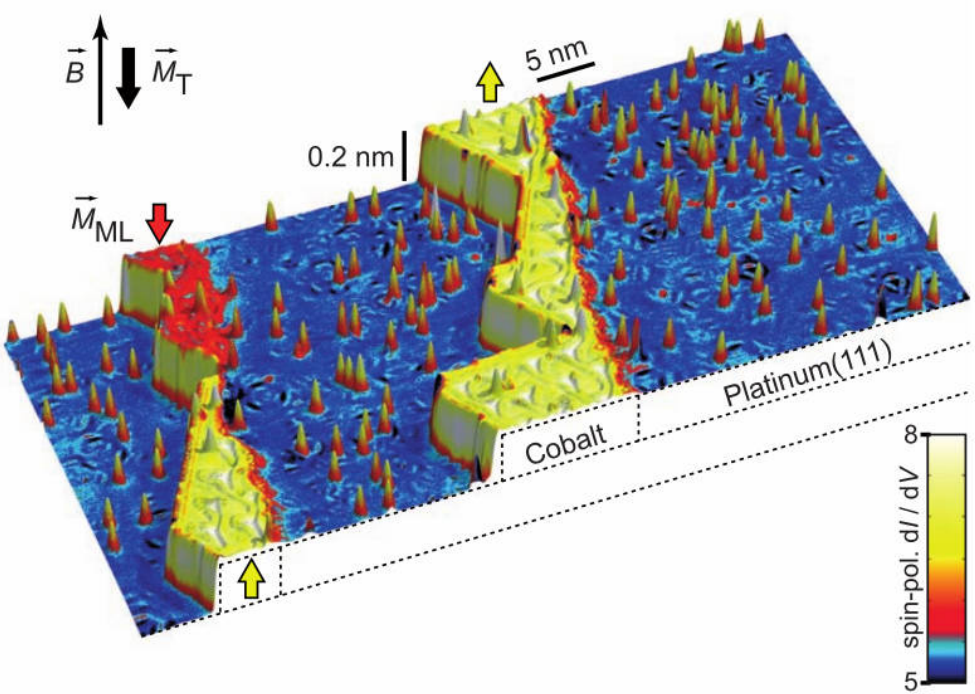

Fig. 1. Overview of the sample of individual Co adatoms on the Pt(111) surface (blue) and Co ML stripes (red and yellow) attached to the step edges (STM topograph colorized with the simultaneously recorded spin-polarized d*I*/d*V* map measured with an STM tip magnetized antiparallel to the surface normal). An external $\vec{B}$ can be applied perpendicular to the sample surface in order to change the magnetization of adatoms $\vec{M}_A$, ML stripes $\vec{M}_{ML}$, or tip $\vec{M}_T$. The ML appears red when $\vec{M}_{ML}$ is parallel to $\vec{M}_T$ and yellow when $\vec{M}_{ML}$ is antiparallel to $\vec{M}_T$. (Tunneling parameters are as follows: $I = 0.8$ nA, $V = 0.3$ V, modulation voltage $V_{mod} = 20$ mV, $T = 0.3$ K.)

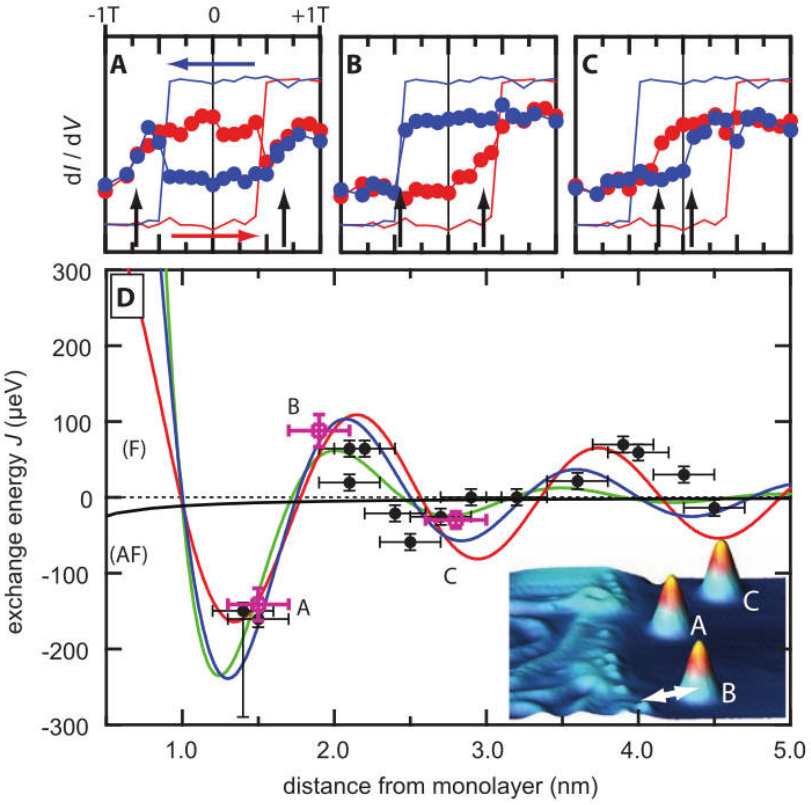

Fig. 4. Magnetic exchange between adatoms and ML stripe. (**A** to **C**) Magnetization curves measured on the ML (straight lines) and on the three adatoms (dots) A, B, and C visible in the inset topograph of (D). The blue color indicates the down sweep from $B = +1$ T to -1 T (and red, the up sweep from -1 T to $+1$ T) (d*I*/d*V* signal on ML inverted for clarity). The vertical arrows indicate the exchange bias field, B_{ex}, which is converted into the exchange energy (using $m = 3.7\mu_B$) for the corresponding magenta points in the plot (D). (Tunneling parameters are as follows: $I = 0.8$ nA, $V = 0.3$ V, $V_{mod} = 20$ mV, $T = 0.3$ K.) (**D**) Dots show measured exchange energy as a function of distance from ML as indicated by the arrow in the inset (about 50° to $[11\bar{2}]$). The black line is the dipolar interaction calculated from the stray field of a 10-nm-wide stripe with saturation magnetization 1.3×10^6 A/m. The red, blue, and green lines are fits to 1D, 2D, and 3D range functions for indirect exchange. Horizontal error bars are due to the roughness of the Co-ML-stripe edge, whereas the vertical ones are due to the uncertainty in B_{ex}.

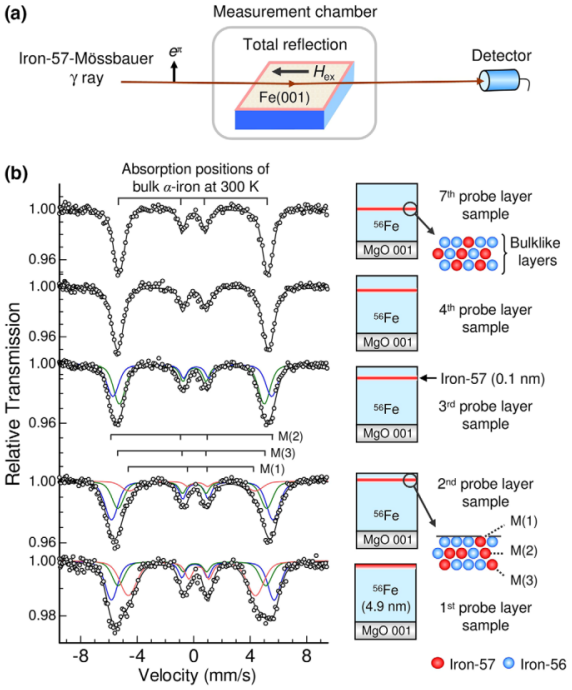

FIG. 1. (a) Experimental setup. e_π, electric field vector of the incident beam; H_{ex}, external magnetic field (300 Oe); detector, NaI(Tl) scintillation detector. (b) Mössbauer spectra of the Nth probe layer samples measured at 300 K. Black solid lines represent the fitted curves. Red, blue, and green lines represent three different magnetic components. $M(i)$ represents the magnetic component assigned to the iron-57 atoms located in the ith layer below the surface.

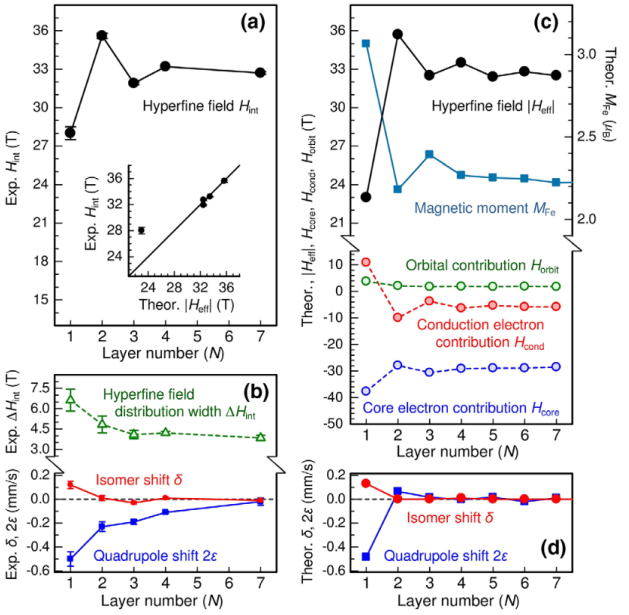

FIG. 2. Plots of the experimental and theoretical layer-by-layer hyperfine parameters. (a) Experimental $H_{\rm int}$ values and experimental $H_{\rm int}$ vs theoretical $|H_{\rm eff}|$ values. (b) Experimental δ, 2ε, and $\Delta H_{\rm int}$ values. (c) Theoretical $M_{\rm Fe}$, $|H_{\rm eff}|$, $H_{\rm core}$, $H_{\rm cond}$, and $H_{\rm orbit}$ values. (d) Theoretical δ and 2ε values. Circles and symbols denote data points. Solid and dashed lines connect data points. In (a) and (b), some uncertainties are less than the size of the data points.

T. Mitsui, S. Sakai, S. Li, T. Ueno, T. Watanuki, Y. Kobayashi, R. Masuda, M. Seto, H. Akai, Phys. Rev. Lett. 125, 236806 (2020)